Acta Biomaterialia 174 (2024) 116–126

Contents lists available at ScienceDirect

Acta Biomaterialia

journal homepage: www.elsevier.com/locate/actbio

Full length article

Chondroitin sulfate, dermatan sulfate, and hyaluronic acid differentially modify the biophysical properties of collagen-based hydrogels

Marcos Cortes-Medina[a], Andrew R. Bushman[b], Peter E. Beshay[c], Jonathan J. Adorno[a], Miles M. Menyhert[b], Riley M. Hildebrand[a], Shashwat S. Agarwal[c], Alex Avendano[a], Alicia K. Friedman[d], Jonathan W. Song[c,e,*]

[a] Department of Biomedical Engineering, The Ohio State University, Columbus OH 43210, USA
[b] Department of Chemical and Biomolecular Engineering, The Ohio State University, Columbus OH 43210, USA
[c] Department of Mechanical and Aerospace Engineering, The Ohio State University, Columbus OH 43210, USA
[d] Department of Chemistry and Biochemistry, The Ohio State University, Columbus OH 43210, USA
[e] The Comprehensive Cancer Center, The Ohio State University, Columbus OH 43210, USA

ARTICLE INFO

Article history:
Received 26 May 2023
Revised 30 November 2023
Accepted 8 December 2023
Available online 14 December 2023

Keywords:
Extracellular matrix
Scaffold
Microstructure
Transport
Microfluidics
Biopolymers
Stiffness

ABSTRACT

Fibrillar collagens and glycosaminoglycans (GAGs) are structural biomolecules that are natively abundant to the extracellular matrix (ECM). Prior studies have quantified the effects of GAGs on the bulk mechanical properties of the ECM. However, there remains a lack of experimental studies on how GAGs alter other biophysical properties of the ECM, including ones that operate at the length scales of individual cells such as mass transport efficiency and matrix microstructure. This study focuses on the GAG molecules chondroitin sulfate (CS), dermatan sulfate (DS), and hyaluronic acid (HA). CS and DS are stereoisomers while HA is the only non-sulfated GAG. We characterized and decoupled the effects of these GAG molecules on the stiffness, transport, and matrix microarchitecture properties of type I collagen hydrogels using mechanical indentation testing, microfluidics, and confocal reflectance imaging, respectively. We complement these biophysical measurements with turbidity assays to profile collagen aggregate formation. Surprisingly, only HA enhanced the ECM indentation modulus, while all three GAGs had no effect on hydraulic permeability. Strikingly, we show that CS, DS, and HA differentially regulate the matrix microarchitecture of hydrogels due to their alterations to the kinetics of collagen self-assembly. In addition to providing information on how GAGs define key physical properties of the ECM, this work shows new ways in which stiffness measurements, microfluidics, microscopy, and turbidity kinetics can be used complementarily to reveal details of collagen self-assembly and structure.

Statement of Significance

Collagen and glycosaminoglycans (GAGs) are integral to the structure, function, and bioactivity of the extracellular matrix (ECM). Despite widespread interest in collagen-GAG composite hydrogels, there is a lack of quantitative understanding of how different GAGs alter the biophysical properties of the ECM across tissue, cellular, and subcellular length scales. Here we show using mechanical, microfluidic, microscopy, and analytical methods and measurements that the GAG molecules chondroitin sulfate, dermatan sulfate, and hyaluronic acid differentially regulate the mechanical, transport, and microstructural properties of hydrogels due to their alterations to the kinetics of collagen self-assembly. As such, these results will inform improved design and utilization of collagen-based scaffolds of tailored composition, mechanical properties, molecular availability due to mass transport, and microarchitecture.

1. Introduction

The composition and assembly of the extracellular matrix (ECM) is vital to the maintenance of tissue as these properties reg-

* Corresponding author.
E-mail address: song.1069@osu.edu (J.W. Song).

https://doi.org/10.1016/j.actbio.2023.12.018
1742-7061/

ulate cell signaling cues and solute and fluid transport [1]. Fibrillar type I collagen is the most abundant protein in the ECM [2]. In addition to collagen, glycosaminoglycans (GAGs) are integral to the structure and function of the ECM and connective tissue [3,4]. GAGs are complex and intrinsically highly negatively charged (or anionic) polysaccharide molecules that can modulate the bioactivity of the ECM through non-covalent interactions with other molecules. Such examples include altering the structural properties of fibrillar collagen [5,6] and locally immobilizing growth factors and chemokines [7] through electrostatic-driven interactions. Some properties of GAGs, such as expression quantity, molecular weight (MW), and post-translational modifications (e.g., changes in sulfation patterns), may be altered in diseased tissue [8].

Among the GAG types, hyaluronic acid (HA), chondroitin sulfate (CS), and dermatan sulfate (DS) are the most prevalent in the body [9]. These GAGs have been shown to be upregulated in pathologies characterized by an overabundance of fibrous connective tissue or desmoplasia such as cancer and fibrosis [10–13]. HA is the only non-sulfated GAG and its disaccharide repeating unit is composed of d-glucuronic acid and N-acetyl-d-glucosamine [14]. Unlike other GAG molecules, whose negative charges are attributed to sulfated groups, the negative charge of HA is due to its d-glucuronic acid groups [15]. The anionic property of HA is conducive for its propensity to imbibe fluid and swell [16,17]. The MW of HA usually exceeds 100 kDa [9,14]. CS contains repeating disaccharide units of d-glucuronic acid and N-acetylgalactosamine. CS and DS are stereoisomers and therefore have similar structures except for the d-glucuronic acid component in CS being changed to l-iduronic acid in DS [18]. Free CS and DS also have comparable ranges for their MWs (CS = 5–50 kDa; DS = 15–40 kDa) [14]. Like HA, the presence of CS and DS in the ECM alters tissue swelling, fluid retention, and cell signaling [19–21]. Unlike HA, CS and DS are found predominantly as chains covalently linked to core proteins to form proteoglycans [19,22].

Reconstituted collagen hydrogels are widely used by tissue engineers, materials scientists, and biologists to recapitulate *in vitro* the physical features of native *in vivo* tissue [23]. Most of the physical and structural properties of collagen hydrogels are controlled by the architecture formed by the mesh of fibers [24,25]. Fiber assembly of collagen is a forward forming entropic reaction that is controlled by pH and temperature [26]. GAGs have also been used to modify the collagen polymerization kinetics and tune the resultant fiber properties of composite hydrogels [23,27,28]. Although HA, CS, and DS have some similar functional characteristics, to our knowledge, it has not been determined experimentally whether these GAG molecules exert distinct changes to the physical and structural properties of collagen matrices. In addition, prior experiments studying the mechanics of collagen-GAG composite gels tend to focus on bulk mechanical properties such as tissue-level stiffness. However, cells respond to fiber level features such as radius, density, alignment, and matrix pore size. These physical properties of the ECM have been shown to mediate cell adhesion, clustering, and cancer cell invasion [29–33]. Recently, our group showed that HA enhances interstitial flow-mediated angiogenic sprouting through its alterations to collagen ECM stiffness and pore size in a microfluidic-based tissue analogue model [34]. This result demonstrates the roles of ECM composition and physical properties in controlling angiogenesis in the presence of biomolecular transport and fluid mechanical stimulation due to interstitial flow. Moreover, this example emphasizes the importance of investigating the collective effects of multiple ECM parameters on cell responses, rather than one aspect in isolation, such as ECM composition or stiffness.

The present study seeks to elucidate how the GAG molecules CS, DS, and HA alter key mechanical, transport, and microstructural properties of collagen hydrogels at a fixed collagen:GAG ratio. We implement an integrated biophysical characterization scheme for hydrogels previously developed by our group to profile and decouple ECM physical properties, including stiffness, hydraulic permeability, and microarchitecture, using mechanical indentation, microfluidics, and confocal reflectance imaging, respectively (Fig. 1). As expected, HA significantly increased the indentation modulus of collagen hydrogels while surprisingly both CS and DS had no effect. Addition of CS, DS, and HA decreased hydraulic permeability of collagen-based hydrogels. Interestingly, while CS and DS had similar effects on stiffness and hydraulic permeability properties of collagen hydrogels, these two stereoisomers exerted significant differences on the collagen matrix pore size, fiber radius, and total fiber count. Moreover, we characterized collagen aggregate formation with turbidity measurements, which revealed that CS, DS, and HA differentially modify collagen polymerization kinetics. These results provide an enhanced understanding of the behavior of collagen assembly in the presence of different GAG constituents. This outcome enables improved design and utilization of collagen-based scaffolds used for tissue engineering of tailored composition, mechanical properties, molecular availability due to mass transport, and microarchitecture.

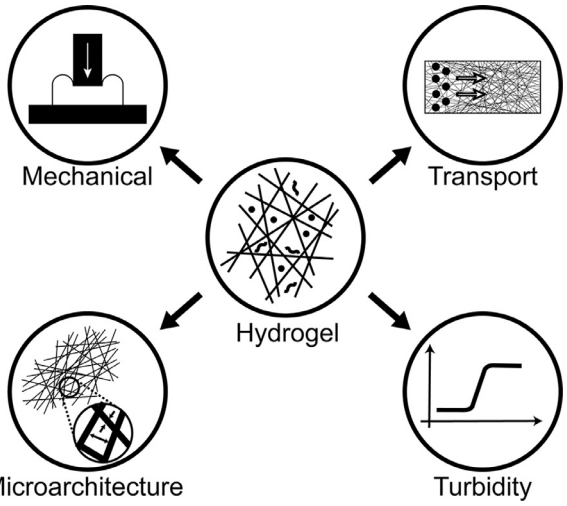

Fig. 1. Characterization scheme for collagen-based hydrogels. Collagen was supplemented with different GAGs (hyaluronic acid, chondroitin sulfate, or dermatan sulfate) and assayed for indentation stiffness (mechanical), hydraulic permeability (transport), confocal reflectance microscopy (microarchitecture), and turbidity (aggregate formation). .

2. Materials and methods

2.1. Preparation and casting of collagen hydrogels

The collagen hydrogels used in the present study were prepared following the manufacturers' instructions. In brief, rat tail type I collagen (300 kDa) stored in acidic solution (Corning Life Sciences) was neutralized to a pH of 7.4 using sodium hydroxide and a 10X phosphate-buffered saline solution. The final concentration of the collagen was then adjusted to 3 mg/ml using Dulbecco's modified Eagle's medium (DMEM). CS (~30 kDa), DS (~30 kDa), and HA (~400 kDa) were acquired from Millipore Sigma. For the GAG supplemented conditions, either CS, DS, or HA were dissolved in sterile water to a concentration of 1 mg/ml and then added to collagen during hydrogel preparation, thereby giving a final collagen-to-GAG ratio of 3:1. This ratio was selected based on previous literature for physiological conditions: one example is the ratio of collagen to HA in breast tumors, which range from 2.4:1 – 7.7:1 [35,36]. Therefore, the collagen to HA ratio used for this study is in

line with levels observed in tumors. After mixing the constituents, the hydrogels were then incubated at 4 °C for 12 min to enhance fiber formation [37]. The incubated collagen-based hydrogels were then injected inside poly(dimethylsiloxane) (PDMS) microchannels that were bonded to glass slides, PDMS wells, or 96 well-plates for their respective assays (Fig. 1). Subsequently, the hydrogels were placed in an incubator (37 °C, 5 % CO_2) for 30 min. Finally, the gels were hydrated with DMEM and returned to incubator conditions for 48 h prior to data acquisition to ensure complete polymerization and equilibrium swelling conditions.

2.2. Stiffness analysis

The mechanical stiffness of the hydrogels was measured after applying a stress-strain relaxation technique adopted from Barocas et al. [38]. Briefly, a mechanical load testing instrument (Electroforce 5500, TA Instrument) was used to indent hydrogels cast in a PDMS well (8 mm diameter; 3 mm in height) at a strain rate of 10 % per second. The indentation was done in a sequence of four incremental indentations—10, 20, 30, and 40 % strain—each followed by a 5-minute period of relaxation. Load readings corresponding to the peaks of 20, 30 and 40 % strain were used to determine indentation stresses while considering the geometry of the indenter. Indentation modulus was calculated after plotting the stresses with their corresponding strain. The data was processed using an in-house MATLAB code. To evaluate the contributions of both the viscous and elastic components of the measured data, the relaxation following each indentation peak was fitted to a viscoelastic model composed of two Maxwell elements (i.e., a spring in series with a dashpot):

$$E^i_{total} = E^0 + E^i_1 e^{-t/\tau_1} + E^i_2 e^{-t/\tau_2} \text{with } \tau_j = \frac{\mu_j}{E^i_j},$$

Where E^i_j are indentation modulus values, τ_j are relaxation time constants, μ_j are viscosity coefficients, and t is the relaxation time (300 s for each step). For each indentation step, E_{total} was computed and then fitted to the viscoelastic model.

2.3. Microfluidic hydraulic permeability measurement

Hydraulic permeability or Darcy's permeability is a characteristic of the matrix that relates interstitial fluid velocity with an applied pressure gradient [39]. This measurement was used to characterize the convective transport properties of the collagen hydrogels. The hydraulic permeability was measured using a rectangular microfluidic device (length: 5 mm; width: 500 μm; height: 1 mm) 48 h post hydrogel polymerization as previously described [27,40]. Briefly, a pressure gradient was created across the channel by fitting a pipet tip filled with DMEM in one port of the microchannel. The hydrostatic pressure gradient generates flow across the hydrogel driven by the height difference between ports. The average velocity of the flow across this channel was then measured by using a fluorescent tracer, 65.5 kDa tetramethylrhodamine isothiocyanate–bovine serum albumin (TRITC-BSA, Millipore Sigma). Time-lapse epifluorescent microscopy images were taken every 5 s for 5–10 min (Nikon TS-100F, equipped with a Q-Imaging QIClick camera). A MATLAB algorithm was then used to estimate the hydraulic permeability (K) of the hydrogels calculated from Darcy's Law:

$$K = \frac{v \times \mu \times \Delta L}{\Delta P},$$

where μ is the viscosity of the fluid (0.001 Pa s), ΔL is the length of the microfluidic channel (5 mm), and ΔP is the hydrostatic pressure gradient across the hydrogel estimated using Pascal's law:

$$\Delta P = \rho \times g \times h,$$

where ρ is the density of the fluid (1000 kg/m^3), g is the acceleration due to gravity (9.81 m/s^2), and h is the fluidic height difference between the microfluidic channel ports.

2.4. Confocal reflectance microscopy for collagen fiber pore size, radius, number, and solid fraction analysis

Confocal reflectance microscopy has been used to observe and characterize the fibers of collagen without the need for fluorescent tagging [24]. Consequently, subtle changes to collagen microarchitecture due to the addition of GAGs can be imaged and quantified [27]. Collagen fibers contained within a PDMS microchannel, were imaged using a Nikon A1R live-cell imaging microscope via a 40×1.3 NA oil immersion lens. Exciting the collagen-based hydrogels with a 487 nm laser and then passing the light through a 40/60 beam splitter allowed a detector to collect the light for visualization of the collagen fibers. Eighty to ninety images were collected per stack, each with a z-step of 0.59 μm.

The acquired confocal reflectance stacks were analyzed using a custom MATLAB code developed by our group [27]. The software determined the fiber radii and pore size of the collagen hydrogels. Fiber radii were measured after skeletonizing the stacks in 3-D using the Skeleton tool of NIH's Image J Software. Total skeleton length was computed to estimate the radius of the fibers. Pore size was estimated using nearest obstacle distance (NOD) method [41].

To measure collagen solid fraction, the confocal z-stacks were binarized and threshold using ImageJ and processed in an in-house MATLAB code. Briefly, the fiber-occupied space was determined as having a pixel value of "one" and any pore or void space was determined as having a "zero" value. For fiber number, a fiber was determined as any object occupying three pixels with a connecting pixel located at any sixteen possible adjacent face (spaces excluded are placed in the diagonal orientation). With the total fiber count and pixel value pertaining to these fibers, solid fraction was determined as the ratio of total pixel volume of fibers to total pixel volume (512×512 x number of stacks).

2.5. Turbidity assay

Turbidity measurements track collagen aggregate formation by particle light scattering, measuring absorbance as clear hydrogel solutions turn opaque during polymerization [28]. Collagen-based hydrogels for turbidity measurements were prepared as described above. Afterwards, 100 µl of hydrogel solution was added to a pre-chilled flat bottom 96-well plate (VWR). The absorbance of the collagen solutions was measured at 400 nm wavelength in an incubated (37 °C) plate reader (Tecan) until the hydrogel polymerized. Separate experiments were conducted to ensure CS, DS, and HA solutions independent of collagen did not lead to noise in the turbidity measurements. Turbidity curves are sigmoidal and can be divided into three segments: 1) lag phase (or nucleation), 2) growth phase, and 3) plateau phase [42]. During the lag phase, turbidity is unchanged while during the growth phase turbidity rapidly increases before a plateau is reached as available collagen is depleted [24].

Turbidity curves were fitted using a sigmoid growth curve

$$F(x) = \frac{L}{1 + e^{-k(x-x0)'}}$$

where x_0 is the sigmoid midpoint, L equals the curve's maximum value, and k is the steepness of the curve. The lag time, inflection time, time to plateau (or plateau time), and the rate of increase in the growth phase (kg), were calculated from the turbidity curves as previously demonstrated [42]. Lag time depicts the start of collagen polymerization and was defined as the point at which the

fit of the first derivative curve increased 5 % over its initial value. Inflection time represents the halfway point of polymerization and was defined as the time associated with the midpoint of the sigmoid curve (i.e., the time of max peak in first derivative curve). Plateau time describes the end of gel formation and was defined as the time at which the first derivative curve reached 95 % of its maximum value, and kg was described as the linear portion between lag time and plateau time (**Supplemental Figure 1**).

$$E^i_{total} = E^0 + E^i_1 e^{-\frac{t}{\tau_1}} + E^i_2 e^{-t/\tau_2}$$

2.6. Circular dichroism spectroscopy

Collagen and collagen-GAG solutions were prepared as hydrogels and loaded on a transmission sample holder. Circular dichroism (CD) spectra were recorded using a J-815 Spectropolarimeter (Jasco Corporation, Japan) at Room temperature (23 °C) with a 2 mm path length in the far UV region (180–240 nm) under nitrogen. All measurements were averaged over 3 repeats with a 4-second data integration time and a 0.5 nm interval. CD data was further analyzed using Beta Structure Selection (or BeStSel), a freely accessible web server for protein secondary structure prediction and fold recognition [43].

2.7. Statistical analysis

Statistical analysis was conducted using analysis of variance (ANOVA) followed by Tukey's post testing for pairwise comparisons between controls and collagen conditions with CS, DS, and HA. All results shown are presented with error bars representing the standard error of the mean (SEM). Each experiment was run with at least technical duplicates, with three sets of biological replicates pooled together for statistical evaluation. A p-value of 0.05 was used as a threshold for statistical significance between results.

3. Results

3.1. Differential modification of the mechanical properties of collagen-based hydrogels by CS, DS, and HA

First, we determined the bulk mechanical properties of the different hydrogel compositions by measuring the peak indentation modulus using methods previously described by our group and others (Fig. 2A-B) [27,38]. The indentation modulus was significantly greater by 2.3-fold for the collagen + HA condition (5.05 kPa) versus the collagen only condition (2.16 kPa) (Fig. 2C). In contrast, the indentation modulus for collagen + CS (2.35 kPa), collagen + DS (2.60 kPa), and collagen only was not statistically different. While both CS, DS, and HA have been shown to resist compressive loading, our results suggest that HA—but not CS and DS—exerts a dominant effect in the resistance to compression when integrated with fibrillar collagen-based hydrogels. Further analysis into the relaxation conditions of the hydrogels via modeling with Maxwell elements (**Supplemental Figure 2**), showed that while GAGs impart different bulk mechanical properties, the materials are all relaxing within the same time scale (**Supplemental Figure 2**). Recently it was reported that the relaxation of hydrogel materials is pivotal in mediating cell motility and adhesion [44]. Notably, collagen + DS and collagen + HA have a higher relaxation load under strain when compared to collagen only conditions [38].

3.2. CS, DS, and HA do not significantly alter the hydraulic permeability of collagen-based hydrogels

Next, we evaluated the convective transport properties of the hydrogels as these are dependent on ECM composition [27]. Mass transport properties (i.e., convection and diffusion) influence cell behavior by controlling physiologically important parameters such as shear stresses, chemical gradients, nutrient availability, and drug delivery [39,45]. Following a protocol developed by our group, a microfluidic device was used to evaluate the effect of CS, DS, or HA on hydraulic permeability of collagen-based hydrogels. Hydraulic permeability is a coefficient that describes the convective transport properties of semiporous medium such as the ECM [46]. The addition of either CS, DS, or HA to collagen hydrogels showed no significant effects on hydraulic permeability when compared to collagen alone (Fig. 3). Previous work from our lab attributed this outcome to the competing effects of increased fiber radius and increased pore size when adding HA to collagen matrices, which nullified any changes in permeability due to increased HA content [27]. This outcome was supported by a past study that demonstrated that a GAG-rich hydrogel led to decreased transport when compared to a collagen-GAG composite hydrogel [47]. In a collagen-GAG scaffold, GAGs such as HA and CS tend to associate around the collagen fibers and become excluded from the interstitial space which may explain the nonsignificant change in permeability.

3.3. Differential effects of CS, DS, and HA on collagen matrix microstructural properties and fiber content

Next, we used confocal reflectance microscopy (Fig. 4A) to quantify how modifications to collagen polymerization kinetics led to differences in the collagen matrix microarchitecture parameters of fiber radius, pore size, solid fraction, and total fibers (Fig. 4B-E). Compared to collagen only, collagen + DS and collagen + HA significantly increased fiber radius by ~22 % (+DS) and 12 % (+HA) (Fig. 4B). Similarly, collagen + DS and collagen + HA increased matrix pore size by 24 % and 15 %, respectively, when compared to collagen only (Fig. 4C). Interestingly, and in contrast to collagen + DS and collagen + HA, collagen + CS had no significant effect in fiber radius (Fig. 4B), yet pore size decreased by 8.0 % (Fig. 4C) compared to the collagen only hydrogel. In Fig. 4D we plot the solid fraction. The volume fraction of solids in fibrillar collagen-based matrices are a property dependent on fiber radius (Fig. 4B), fiber length, and number of fibers. When compared to the collagen only condition, collagen + CS and collagen + DS had no significant effect on the solid fraction. In contrast, collagen + HA had a significant decrease of ~ 20 % in solid fraction compared to collagen only (Fig. 4D). In Fig. 4E, we plot the total fiber count per z-stack as a measure of the number of fibers. The collagen + CS matrix condition significantly increased total fibers by ~ 14 % when compared to the collagen only condition (Fig. 4E). In contrast, when compared to collagen only, collagen + DS and collagen + HA significantly decreased total fiber count by 35 % and 17 %, respectively. Interestingly, none of the modifications had effects on fiber alignment (**Supplemental Figure 3**). Notably, of the experimental conditions, collagen + DS demonstrated the largest percent change in fiber radius, pore size, and total fibers compared to the collagen only condition.

3.4. CS, DS, and HA differentially influence the rate of collagen polymerization

Next, we employed a turbidity assay to evaluate how GAG supplementation affects the polymerization dynamics of collagen matrices by measuring optical density (OD) over time (Fig. 5A). Interestingly, while the maximum ODs during the plateau phase for the collagen + CS, and collagen + DS conditions were within +/- 2.2 % of the collagen only condition, the OD for the collagen + HA condition was ~ 13 % lower than the collagen only condition (Fig. 5A). This outcome suggests that the collagen + HA condition has less

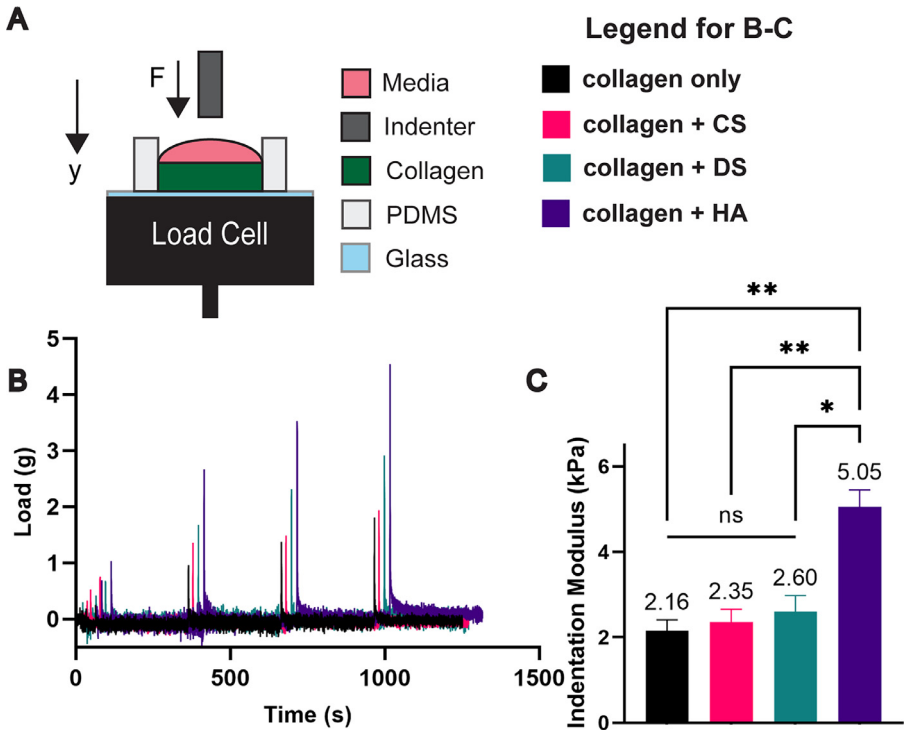

Fig. 2. Differential effects of CS, DS, and HA in altering hydrogel stiffness. A) Collagen solutions are cast on a PDMS well and subjected to stresses using indentation. B) Sample load readings of tested conditions. C) Only HA laden hydrogels led to increases in stiffness. Error bars denote SEM; NS is non-significant, $^{*}<0.05$, $^{**}<0.01$.

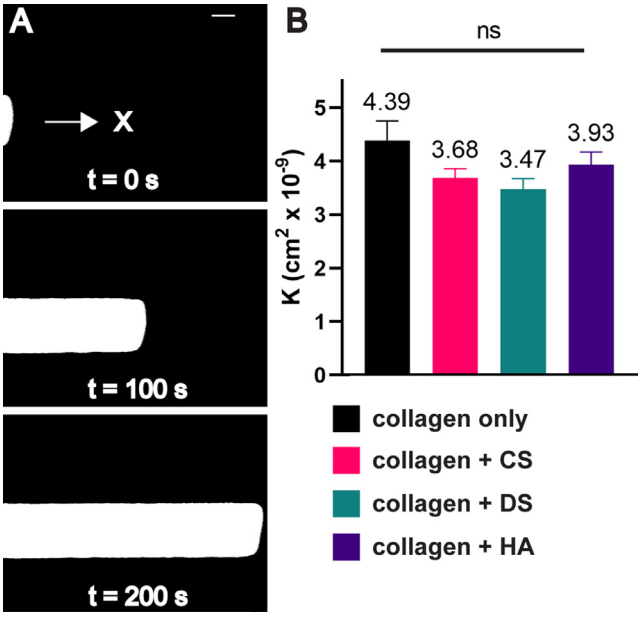

Fig. 3. Hydraulic permeability measurements of GAG modified collagen matrices. A) Time-lapse microscopy is used to track a TRITC dye in a microfluidic channel to obtain the velocity of the flow. B) The addition of HA, CS, or DS does not decrease hydraulic permeability (K). Scale bar = 200 μm. Error bars denote SEM. NS is non-significant ANOVA for all conditions tested.

total polymerized collagen fiber content compared to other experimental conditions. This result also agrees with the solid fraction (Fig. 4D) and total fiber calculations (Fig. 4E). Further analysis of the polymerization kinetics showed that collagen + CS did not change the lag time statistically compared to collagen only (Fig. 5B), but significantly decreased the inflection time (495 s versus 577 s, Fig. 5C) and the plateau time (759 s versus 907 s, Fig. 5D, **Supplemental Figure 4**). In contrast, when compared to collagen only, collagen + DS significantly decreased the lag time (296 s versus 348 s) and the inflection time (529 s versus 577 s) but did not change the plateau time (Fig. 5B-**D**). Our results with CS and DS are in accordance with previous studies, which have shown that CS modifies collagen fiber microstructural properties [48,49].

Compared to the collagen only condition, collagen + HA significantly increased the lag time (420 s versus 348 s) but did not change the inflection and plateau times (Fig. 5B-**D, Supplemental Figure 4**). The observation that HA delays the lag phase of collagen polymerization agrees with previous results, which suggested that HA sterically impedes the aggregation of collagen molecules during self-assembly [4]. Interestingly, collagen + CS resulted in a significant increase in the growth phase (kg), compared to collagen only, collagen + DS, and collagen + HA conditions (**Supplemental Figure 1**). These outcomes suggest that CS but not DS and HA promotes more rapid collagen fibrillogenesis compared to collagen only conditions [50].

3.5. CS, DS, and HA differentially alter the spectroscopic signal of collagen

Circular dichroism (CD) spectroscopy is primarily used to investigate the secondary structures of proteins [51]. It has been reported that fibrillar type I collagen has a unique CD spectral signature of a strong negative ellipticity band between 200 and 210 nm and a positive peak between 220 and 230 nm [52]. The negative band corresponds with collagen fibrillogenesis while the positive peak is associated with the canonical triple helical structure of collagen [52]. Here we report changes in CD spectral shapes of collagen due to the addition of the different GAGs. As expected, for the collagen only condition we observed a negative spectral band between 200 and 210 nm and a positive spectral peak between 220 and 230 (Fig. 6A). For the different collagen + GAG conditions, we observed differential shifts, both in the amplitude and

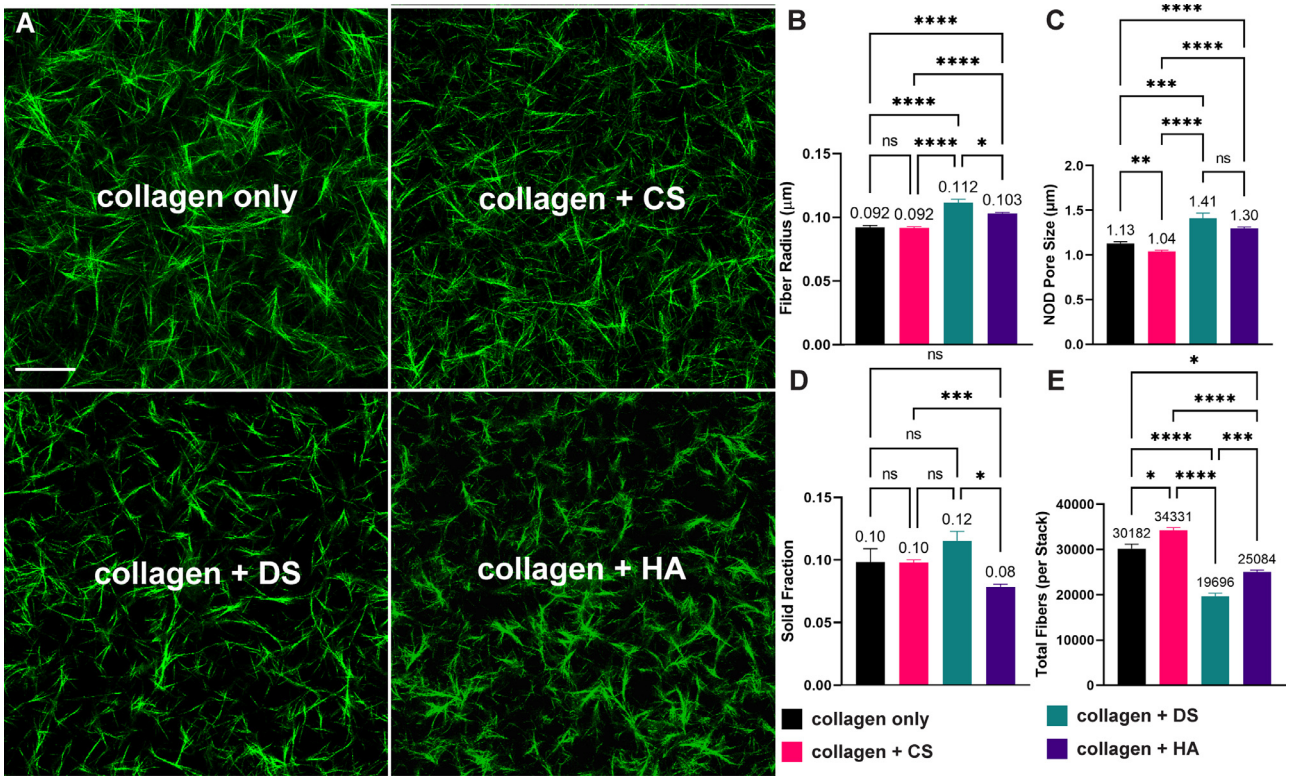

Fig. 4. Microstructural analysis of collagen-based hydrogels. HA and DS increase both matrix pore size and fiber radius, while CS leads to decrease in fiber pore size. A) Representative images of collagen fibers. B-C) Addition of DS and HA leads to increases in pore size and radius. D) HA decreased the solid fraction following processing of confocal images. E) DS and HA decreased the number of collagen fibers, while CS led to increased amounts of fibers when compared to collagen only. Scale bar = 50 μm. Error lines represent the SEM. Statistical significance denoted as NS is non-significant, * <0.05, ** <0.01, *** <0.001, **** < 0.0001.

the wavelength, at which the negative bands and positive peaks occur (Fig. 6A). The CD spectra data was further analyzed with BeStSel [43](see Materials and Methods) to determine the percentage of common protein secondary structure elements, including alpha helix (Fig. 6B), beta sheet (Fig. 6C), turn (Fig. 6D), and unordered (Fig. 6E). Fig. 6B–E show that the CS, DS, and HA modify the collagen protein secondary structures differentially. Compared to collagen only, collagen + HA significantly increased the alpha helix content and decreased the beta sheet and unordered structures. Collagen + DS increased the unordered structures significantly and decreased beta sheet structures when compared to collagen only. Additionally, DS modestly increased the alpha helix content of collagen, but this change was not significant. Collagen + CS significantly decreased beta sheet content and increased the unordered structures compared to collagen only. All three of the GAGs studied failed to alter the composition of turn structures when compared to collagen only.

4. Discussion

In the design and utilization of hydrogels for cell culture and tissue engineering applications, it is essential to characterize the properties that influence the compositional, mechanical, and structural cues to cells. In this study, we quantified the biophysical properties of collagen-based hydrogel systems using an integrated approach that enabled independent measurements of key mechanical, transport, and microarchitectural characteristics. Our studies focused on hydrogels comprised of physiological collagen-to-GAG ratios. For all experiments, we used a fixed collagen concentration (3 mg/ml) and compared outcomes of the addition of three different GAG types (CS, DS, and HA) that were also added at a fixed concentration (1 mg/ml). Our results provide a uniquely detailed understanding of how the addition of different GAG types differentially alter collagen polymerization kinetics that translate to distinct physical and structural properties of the ECM. These results will aid researchers who aim to better understand the combined biological effects of multiple ECM parameters, such as composition and biophysical properties, on cell behavior and function.

Turbidity measurements enable temporal distinctions between the collagen and GAG conditions during hydrogel polymerization. The optical density of the absorbance measurements that correspond to the plateau in the sigmoid turbidity curves relates to the total collagen content present in fibril form [53]. Our turbidity measurements are supported by the microstructural features and the collagen solid fraction present in the matrices studied. For instance, the inflection and plateau times for collagen + CS were significantly decreased compared to collagen only. This result suggests that the addition of CS accelerated total collagen polymerization. More rapid collagen fibrillogenesis and fiber count due to CS addition is further supported by increased kg during the growth phase (i.e., a greater slope between the plateau and lag time of the sigmoidal curve). Examining the microstructural features, the significant increased total fiber count for collagen + CS, compared to collagen only, also suggests that CS enhances collagen fibrillogenesis. Thus, for collagen + CS, we observed increased fiber content with reduced pore size and no change in fiber radius compared to collagen only, which suggests that the addition of CS modifies the length of collagen fibers or the total number of pores.

For the collagen + DS condition turbidity measurements, we observed decreased lag and inflection time compared to collagen only. Shifts to the left of the sigmoid curve have been reported to be associated with accelerated fibrillogenesis [28], which corresponds with fibril thickening [42]. This outcome is supported by the microarchitecture analysis for collagen + DS, where we ob-

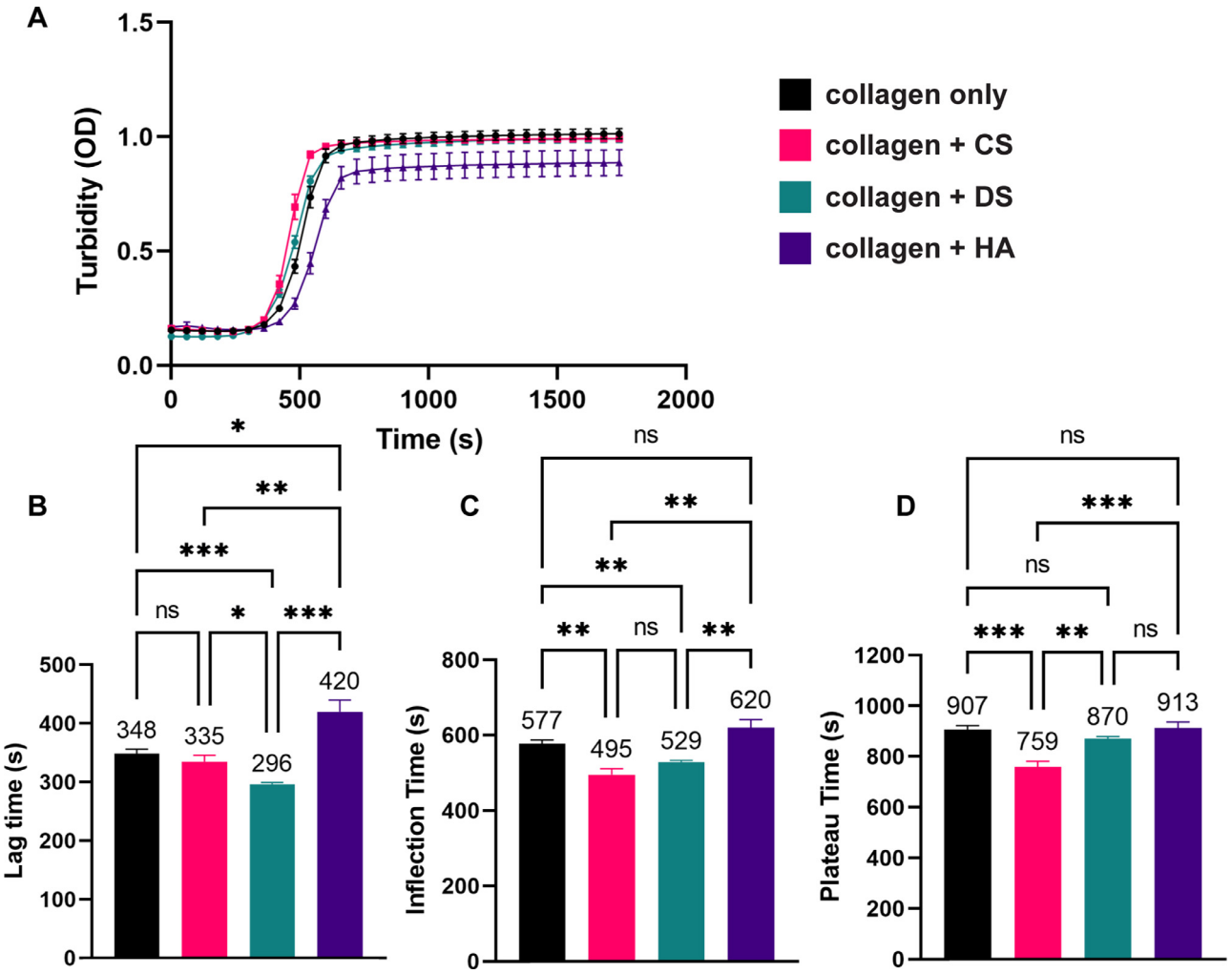

Fig. 5. Turbidity measurements of collagen gel solutions. A) Addition of GAGs differentially affects the rate of collagen fibril polymerization in terms of B) Lag time, C) Inflection time, and D) Plateau time. While CS and DS enhance the rate of collagen fibril formation, HA hinders the rate of polymerization. Error lines represent the SEM ($n > 9$ per condition). Statistical significance denoted as NS is non-significant, $^{*}<0.05$, $^{**}<0.01$, $^{***}<0.001$.

served increased radius, and collagen solid fraction. Of the experimental conditions, collagen + DS exhibited the largest percent changes compared to collagen only for the microstructural parameters of fiber radius, pore size, and total fiber count. These results suggest that the strengths in interactions between collagen and DS manifest in quantifiable changes in microstructural properties of the resulting collagen fiber network. Several studies have investigated GAG-protein interactions, including GAG-collagen interactions, using spectroscopy analysis [5,54,55]. It is believed that l-iduronic acid containing GAGs (DS and heparan sulfate) interact more strongly with proteins than GAGs lacking l-iduronic acid (CS, HA, and keratan sulfate) [56,57]. Specific to collagen, the conformational flexibility afforded by l-iduronic acid residues facilitate bridging of anionic GAG molecules to basic, cationic regions of nearby collagen molecules [54,57].

In the collagen + HA condition, although the addition of HA delays the start of collagen polymerization, the ratio between plateau time and lag time is comparable to CS, which has the most rapid polymerization of the conditions tested. These results suggest that while HA can sterically impede the start of collagen aggregation and bundling, once hydrogel polymerization initiates, the process accelerates. It is important to note that while HA increases fiber radius—denoting enhanced polymerization—it also decreases the total number of fibers, which can explain why less time is needed for the hydrogel to fully polymerize. Recently, Martin et al., described the effects of the simple monosaccharides d-glucuronic acid, N-acetyl-d-glucosamine, and d-galactose in modifying collagen assembly [58]. This study observed that either the presence of amide groups, or the charged nature of carboxylate groups associated with the sugars (D-glucuronic acid), interact with water molecules on the surface of collagen monomers, thereby increasing the entropy change necessary for spontaneous collagen assembly. While this study did not investigate complete GAG chains, the results provide a plausible explanation for the delay in collagen fibrillogenesis in the presence of HA. Since HA is composed of repeated N-acetyl-d-glucosamine and d-glucuronic acid chains, the molecule is having a similar effect on collagen self-assembly compared to isolated sugars. Future work can focus on the entropy changes caused by the addition of sulfated GAG chains like CS or DS that impart a more negative charge [18,59,60], or the steric exclusion effects of HA of different MWs and of the same charge density [61], to fully understand the influence of GAGs on the kinetics of collagen assembly.

Structurally, CS, DS, and HA are similar anionic polysaccharides. CS is known to have a higher water retaining capacity than HA, leading to ECM with significant swelling that contributes to load-bearing behavior of CS-rich tissue such as cartilage [59,62]. However, of the conditions tested, only collagen + HA hydrogels exhib-

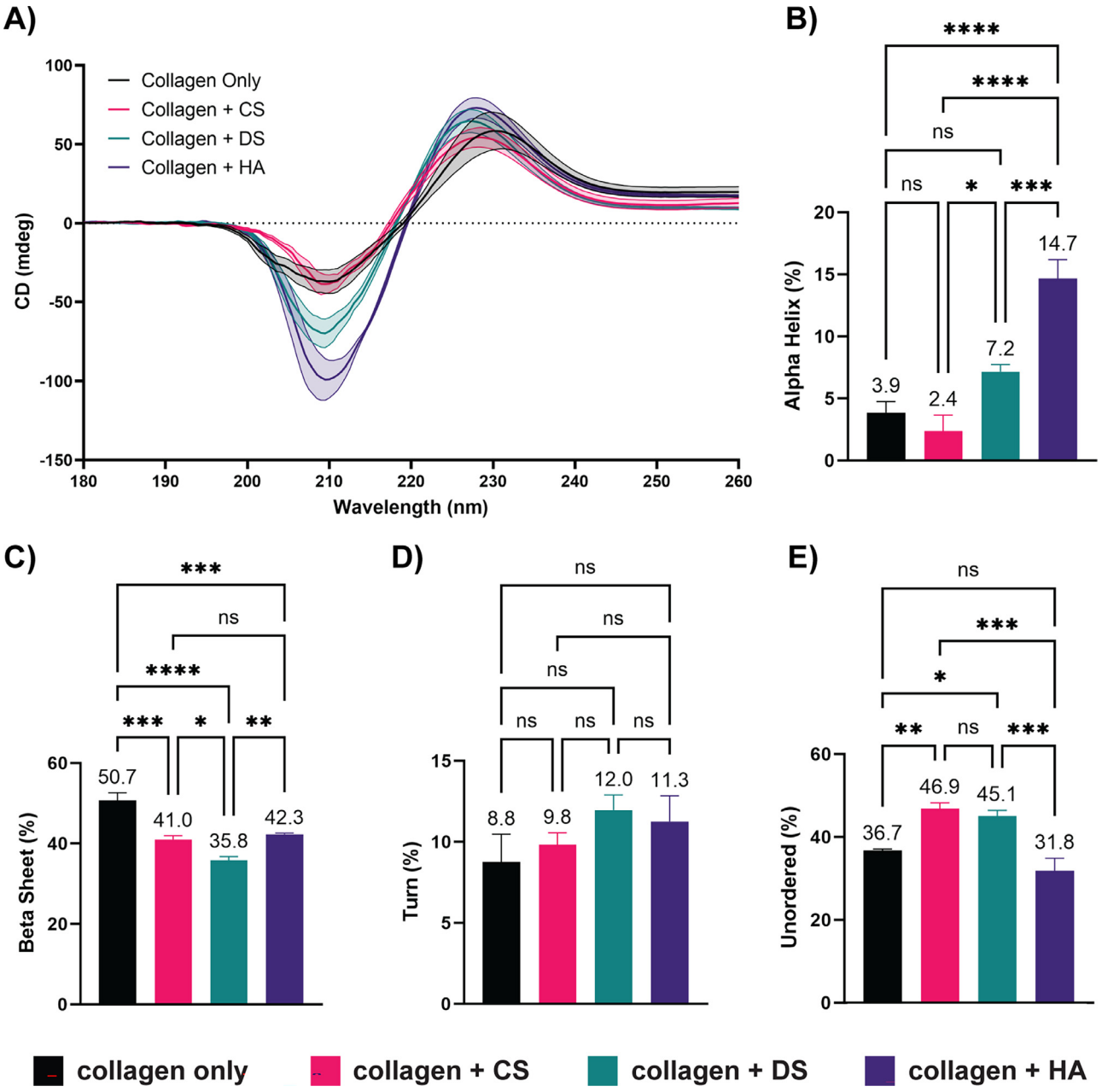

Fig. 6. Circular dichroism spectroscopy of collagen gel solutions. A) CS, DS, and HA produce distinct circular dichroism (CD) spectral signatures for collagen. CD spectra were collected from 180 nm to 260 nm wavelengths. Relative abundance of secondary structures, including B) Alpha Helix, C) Beta Sheet, D) Turn, and E) Unordered. Secondary structure information was generated using the BeStSel Tool (see Materials and Methods).

ited increased indentation modulus. Interestingly, this result was not contingent on the solid collagen fiber fraction as the addition of HA led to decreases in both collagen solid fraction and total fiber count. Our data suggests that HA promotes resistance to compression presumably due to sustained swelling while being indented. For CS and DS, the collagen solid fraction increased when compared to HA; however, this failed to correlate with any changes to the indentation modulus. As CS, DS, and HA cause swelling in collagen matrices, it was unexpected that only HA would lead to significant increases of the indentation modulus with no discernable link between fiber radius, total fiber count, and solid fraction. Nevertheless, it is notable that a previous study showed that enzymatic degradation of CS with chondroitinase did not change the compressive modulus of a collagen-CS gel [63]. In contrast, cleaving HA with hyaluronidase significantly reduced the compressive modulus of a collagen-HA gel to the level of a collagen only [27,34]. Degradation of HA with hyaluronidase results in fragments of HA that are often less than 50 kDa and of comparable MW to free CS and DS [64]. A recent study showed that enhancement of collagen stiffness by HA is a MW-dependent process since the incorporation of lower MW HA fragments (10–20 kDa) into the ECM did not increase the stiffness of a 2 mg/ml collagen + 2 mg/ml HA hydrogel [65]. In contrast, the addition of 100–150 kDa HA to collagen led to significant increases in stiffness of the composite hydrogel [65]. Collectively, these results suggest that additional factors may influence the mechanical behavior of collagen-GAG composite hydrogels: either experimental parameters (e.g., strain rate or level of confinement) or properties of the material tested (e.g., MW of GAG constituent or degree of cross-linking of the biopolymer networks) [59].

CD spectroscopy is a technique widely used in biochemistry to study the structure and interaction of proteins [52,66]. While CD spectroscopy has been used to study the unique fibril spectrum of the different assembly stages and secondary structures of standalone collagen solutions [52], here we present CD as a modality for studying how GAGs modify the CD spectra of collagen. We observed that CS, DS, and HA produce unique spectroscopic signals for collagen, which suggests that these GAGs affect the stability and the secondary structures of collagen. It is increasingly evident that the coupling of collagen-GAG interactions with hydration forces leads to changes in the physical properties of the hydrogels like pore size and modulus. For the collagen + HA condition, we observed a unique CD spectral signal that resulted in a significant and pronounced increase in alpha helix structures compared to collagen only, collagen + CS, and collagen + DS conditions. With our biophysical measurements, we also observed that collagen + HA was the only experimental condition that produced an increase in modulus while also decreasing pore size. Thus, combining CD spectroscopy with our biophysical characterization scheme enables unique insights into how protein secondary structures and molecular interactions may mediate the physical properties of different collagen-GAG hydrogels.

Hydraulic permeability correlates to the drag imparted by the solid compartment of the ECM, with both fibrous and nonfibrillar components contributing to hydraulic resistance [39]. Carman-Kozeny and Happel describe hydraulic permeability further in terms of the geometry of the channel, the overall porosity, and the hydraulic radius of the ECM pores, all of which play a role in defining permissiveness to fluid flow through semiporous matrices [39,67,68]. For the collagen + HA condition, although pore size and fiber radius increased, the solid fraction and total fiber count decreased; these competing effects help explain no net change in bulk hydraulic permeability of the gel. Similarly, DS led to increased pore size and collagen fiber radius, with decreased total fiber count; however, solid fraction increased with DS suggesting that there could be excess drag associated with increased collagen content (either by a reduction in the number of pores or by increased fiber length). In contrast, CS decreased pore size and affected no change in fiber radius nor solid fraction compared to the collagen only condition. Moreover, in a developing biopolymer network, GAGs may associate around individual collagen fibers instead of occupying the interstitial space [47]. Therefore, while it is surprising that the addition of various GAGs did not affect overall hydraulic permeability, all GAG-laden conditions modulated at least one fiber property tied to hydraulic permeability.

Despite observing no significant changes in hydraulic permeability of the hydrogel conditions tested, we believe that these findings will still be very useful for experimental studies that focus on the effects of ECM GAGs on cellular responses, especially when combined with other biophysical measurements such as microstructural analysis. For instance, increases in the mean pore size of collagen only matrices may facilitate cancer cell invasion [29]. In addition, collagen fibers that define the pore size are sufficiently deformable to support angiogenic sprouting of endothelial cells [69,70]. Thus, our findings suggest that the significant increases in collagen matrix pore size due to HA or DS addition may facilitate the initial extension and sustained elongation of multicellular processes into matrix void spaces during cancer invasion or endothelial sprouting. Indeed, we previously reported that the addition of HA to collagen ECM promoted angiogenesis in a microfluidic-based model, however only in the presence of convective interstitial flow [34]. Thus, modifications in the matrix pore size due to HA resulted in changes in interstitial flow induced-shear stress on endothelial cells, which promoted angiogenic sprouting.

In the present study, we observed opposing effects of CS and DS on collagen matrix pore size that are independent of changes in ECM stiffness. This novel finding points to future studies that compare the roles of these two GAG stereoisomers on multicellular cancer cell invasion and angiogenic sprouting. Also of interest are the effects of CS and DS in the presence of interstitial flow as flow-induced shear stress in a 3-D ECM strongly depends upon matrix pore size [71]. The utility of the hydraulic permeability measurements is that we can conclude that these changes observed in endothelial sprouting were not dependent on changes in nutrient limitation, since hydraulic permeability was unchanged with the addition of HA. Like HA, CS and DS have been shown to be upregulated in diseased tissue, such as cancer, atherosclerosis, and fibrosis [72]. Thus, we believe that the findings from this study will be instrumental for gaining a more complete understanding of the contributions of the myriad of instructional cues to cells encoded by collagen ECM enriched with GAGs, especially in the presence of interstitial flow conditions.

We anticipate that the integrated characterization scheme for hydrogels presented here will have broad application for cell culture and tissue engineering studies, especially ones using collagen-based matrices. For example, we can readily characterize the biophysical, solid fraction, and turbidity properties of collagen-based matrices whose stiffness is modified independent of collagen concentration using methods such as enzymatic or chemical crosslinking [73], non-enzymatic glycosylation (or glycation) [74], or non-enzymatic cross-linking of collagen/alginate hybrid gels [75]. Moreover, we can also study modified collagen-GAG composite materials, such as ones that utilize commercially available methacrylated collagen and HA for covalent crosslinking used to slow down hydrogel degradation and enhance mechanical tunability [32,76]. However, it is known that HA methacrylation not only changes hydrogel bioactivity but alters collagen microstructure [77]. To our knowledge, such collagen-based matrices have not been widely deployed in microfluidic systems that combine controlled perfusion and interstitial flow with real-time monitoring of cellular microenvironments [46]. Thus, the approaches described here would help position researchers to investigate the interplay between mechanical and transport factors mediated by interstitial flow and ECM in orchestrating biological function.

5. Conclusions

In this study, we employed an experimental framework that described the effects of the GAG molecules CS, DS, and HA in differentially modifying the properties of collagen-based matrices. Here, we find that the GAGs interact with the collagen fibers during polymerization that manifest in distinct ECM biophysical properties. We observed significantly different effects of CS and DS on the radius of collagen fibers, matrix pore size, and total fiber count. The distinctions between these two GAG stereoisomers on ECM physical properties would not have been revealed if the studies were limited to indentation and microfluidic hydraulic permeability measurements only. Thus, the addition of different GAGs not only alters the bioactivity of collagen-based matrices, but also changes the mechanical and structural properties that define the preconditions for ECM-cell interactions. Our comprehensive and quantitative experimental platform for characterizing the structural, mechanical, and optical properties of biopolymer networks enables a more precise understanding of the polymerization dynamics of collagen-GAG composite hydrogels. Taken together, these results facilitate an enhanced design of biomaterials for cell culture and tissue engineering applications. Moreover, studies detailing the interrelation between compositional, microarchitectural, and mechanical properties will allow for a fuller understanding of how cells and biophysical environments of the ECM function an integrated system to influence cell and tissue behavior and response.

Declaration of Competing Interest

The authors declare that they have no known competing financial interests or personal relationships that could have appeared to influence the work reported in this paper.

Acknowledgements

The authors acknowledge support from an NSF CAREER award (CBET-1752106), the Mark Foundation for Cancer Research (18-024-ASP), the National Heart Lung Blood Institute (R01HL141941), and The Ohio State University Materials Research Seed Grant Program, funded by the Center for Emergent Materials, an NSF-MRSEC, grant DMR-1420451, the Center for Exploration of Novel Complex Materials, and the Institute for Materials Research. Two of the authors (P.E.B. and M.M.M.) gratefully acknowledge funding from the OSU (Ohio State University) Pelotonia fellowship program. One of the authors (M.C-M.) thanks the support from an OSU Graduate Enrichment Fellowship, a Discovery Scholars Fellowship, and an NHLBI Graduate Diversity Supplement. J.J.A is supported by funding from the GEM Fellowship, a OSU Discovery Scholars Fellowship, and the Gates Millennium Scholarship. S.S.A is funded through a University Fellowship and a Distinguished University Fellowship from the OSU Graduate School. This work was also supported, in part, by the Mary Wieczynski Furnivall Cancer Research Fund. Reflectance confocal microscopic images of collagen-based matrices presented in this report were generated using instruments and services at the Campus Microscopy and Imaging Facility (CMIF), The Ohio State University. This facility is supported in part by grant P30 CA016058, National Cancer Institute. Circular dichroism studies were performed in the OSU Biophysical Interaction and Characterization Facility (BICF), which is supported by the OSU Department of Chemistry and Biochemistry. We thank Jacob Holter for critical review of this manuscript.

Supplementary materials

Supplementary material associated with this article can be found, in the online version, at doi:10.1016/j.actbio.2023.12.018.

References

[1] C. Frantz, K.M. Stewart, V.M. Weaver, The extracellular matrix at a glance, J. Cell Sci. 123 (Pt 24) (2010) 4195–4200.
[2] R.O. Hynes, The extracellular matrix: not just pretty fibrils, Science 326 (5957) (2009) 1216–1219.
[3] X. Chen, D. Chen, E. Ban, K.C. Toussaint, P.A. Janmey, R.G. Wells, V.B. Shenoy, Glycosaminoglycans modulate long-range mechanical communication between cells in collagen networks, Proc. Natl. Acad. Sci. U. S. A. 119 (15) (2022) e2116718119.
[4] X. Xin, A. Borzacchiello, P.A. Netti, L. Ambrosio, L. Nicolais, Hyaluronic-acid-based semi-interpenetrating materials, J. Biomater. Sci. Polym. Ed. 15 (9) (2004) 1223–1236.
[5] H. Munakata, K. Takagaki, M. Majima, M. Endo, Interaction between collagens and glycosaminoglycans investigated using a surface plasmon resonance biosensor, Glycobiology 9 (10) (1999) 1023–1027.
[6] M. Raspanti, M. Viola, A. Forlino, R. Tenni, C. Gruppi, M.E. Tira, Glycosaminoglycans show a specific periodic interaction with type I collagen fibrils, J. Struct. Biol. 164 (1) (2008) 134–139.
[7] H. Crijns, V. Vanheule, P. Proost, Targeting chemokine-glycosaminoglycan interactions to inhibit inflammation, Front. Immunol. 11 (2020) 483.
[8] Q. Wang, L. Chi, The alterations and roles of glycosaminoglycans in human diseases, Polymers 14 (22) (2022) 5014.
[9] M. Ennemoser, A. Pum, A. Kungl, Disease-specific glycosaminoglycan patterns in the extracellular matrix of human lung and brain, Carbohydr. Res. 511 (2022) 108480.
[10] D. Jiang, J. Liang, P.W. Noble, Hyaluronan as an immune regulator in human diseases, Physiol. Rev. 91 (1) (2011) 221–264.
[11] M. Liu, C. Tolg, E. Turley, Dissecting the dual nature of hyaluronan in the tumor microenvironment, Front. Immunol. 10 (2019) 947.
[12] K.N. Sugahara, T. Hirata, T. Tanaka, S. Ogino, M. Takeda, H. Terasawa, I. Shimada, J. Tamura, G.B. ten Dam, T.H. van Kuppevelt, M. Miyasaka, Chondroitin sulfate E fragments enhance CD44 cleavage and CD44-dependent motility in tumor cells, Cancer Res. 68 (17) (2008) 7191–7199.
[13] A.D. Theocharis, M.E. Tsara, N. Papageorgacopoulou, D.D. Karavias, D.A. Theocharis, Pancreatic carcinoma is characterized by elevated content of hyaluronan and chondroitin sulfate with altered disaccharide composition, Biochim. Biophys. Acta 1502 (2) (2000) 201–206.
[14] N.S. Gandhi, R.L. Mancera, The structure of glycosaminoglycans and their interactions with proteins, Chem. Biol. Drug Des. 72 (6) (2008) 455–482.
[15] D. Soares da Costa, R.L. Reis, I. Pashkuleva, Sulfation of glycosaminoglycans and its implications in human health and disorders, Annu. Rev. Biomed. Eng. 19 (1) (2017) 1–26.
[16] V.K. Lai, D.S. Nedrelow, S.P. Lake, B. Kim, E.M. Weiss, R.T. Tranquillo, V.H. Barocas, Swelling of collagen-hyaluronic acid co-gels: an in vitro residual stress model, Ann. Biomed. Eng. 44 (10) (2016) 2984–2993.
[17] M. Proestaki, M. Sarkar, B.M. Burkel, S.M. Ponik, J. Notbohm, Effect of hyaluronic acid on microscale deformations of collagen gels, J. Mech. Behav. Biomed. Mater. 135 (2022) 105465.
[18] M. Bathe, G.C. Rutledge, A.J. Grodzinsky, B. Tidor, A coarse-grained molecular model for glycosaminoglycans: application to chondroitin, chondroitin sulfate, and hyaluronic acid, Biophys. J. 88 (6) (2005) 3870–3887.
[19] A. Barkovskaya, A. Buffone Jr., M. Zidek, V.M. Weaver, Proteoglycans as mediators of cancer tissue mechanics, Front. Cell Dev. Biol. 8 (2020) 569377.
[20] E.H. Han, S.S. Chen, S.M. Klisch, R.L. Sah, Contribution of proteoglycan osmotic swelling pressure to the compressive properties of articular cartilage, Biophys. J. 101 (4) (2011) 916–924.
[21] R. Hua, Q. Ni, T.D. Eliason, Y. Han, S. Gu, D.P. Nicolella, X. Wang, J.X. Jiang, Biglycan and chondroitin sulfate play pivotal roles in bone toughness via retaining bound water in bone mineral matrix, Matrix Biol. 94 (2020) 95–109.
[22] D. Struck, W. Lennarz, The Biochemistry of Glycoproteins and Proteoglycans, by WJ Lennarz, Plenum, New York, 1980, pp. 35–83.
[23] V.A. Patil, K.S. Masters, Engineered collagen matrices, Bioengineering 7 (4) (2020).
[24] Y.L. Yang, L.J. Kaufman, Rheology and confocal reflectance microscopy as probes of mechanical properties and structure during collagen and collagen/hyaluronan self-assembly, Biophys. J. 96 (4) (2009) 1566–1585.
[25] B. Sun, The mechanics of fibrillar collagen extracellular matrix, Cell Rep. Phys. Sci. 2 (8) (2021) 100515.
[26] E.E. Antoine, P.P. Vlachos, M.N. Rylander, Tunable collagen I hydrogels for engineered physiological tissue micro-environments, PLoS One 10 (3) (2015) e0122500.
[27] A. Avendano, J.J. Chang, M.G. Cortes-Medina, A.J. Seibel, B.R. Admasu, C.M. Boutelle, A.R. Bushman, A.A. Garg, C.M. DeShetler, S.L. Cole, J.W. Song, Integrated biophysical characterization of fibrillar collagen-based hydrogels, ACS Biomater. Sci. Eng. 6 (3) (2020) 1408–1417.
[28] D. Chen, L.R. Smith, G. Khandekar, P. Patel, C.K. Yu, K. Zhang, C.S. Chen, L. Han, R.G. Wells, Distinct effects of different matrix proteoglycans on collagen fibrillogenesis and cell-mediated collagen reorganization, Sci. Rep. 10 (1) (2020) 19065.
[29] J. Tien, U. Ghani, Y.W. Dance, A.J. Seibel, M.C. Karakan, K.L. Ekinci, C.M. Nelson, matrix pore size governs escape of human breast cancer cells from a microtumor to an empty cavity, iScience 23 (11) (2020) 101673.
[30] J. Sapudom, S. Rubner, S. Martin, T. Kurth, S. Riedel, C.T. Mierke, T. Pompe, The phenotype of cancer cell invasion controlled by fibril diameter and pore size of 3D collagen networks, Biomaterials 52 (2015) 367–375.
[31] C. Liu, B. Chiang, D. Lewin Mejia, K.E. Luker, G.D. Luker, A. Lee, Mammary fibroblasts remodel fibrillar collagen microstructure in a biomimetic nanocomposite hydrogel, Acta Biomater. 83 (2019) 221–232.
[32] A.J. Berger, K.M. Linsmeier, P.K. Kreeger, K.S. Masters, Decoupling the effects of stiffness and fiber density on cellular behaviors via an interpenetrating network of gelatin-methacrylate and collagen, Biomaterials 141 (2017) 125–135.
[33] X. Gong, J. Kulwatno, K.L. Mills, Rapid fabrication of collagen bundles mimicking tumor-associated collagen architectures, Acta Biomater. 108 (2020) 128–141.
[34] C.W. Chang, H.C. Shih, M.G. Cortes-Medina, P.E. Beshay, A. Avendano, A.J. Seibel, W.H. Liao, Y.C. Tung, J.W. Song, Extracellular matrix-derived biophysical cues mediate interstitial flow-induced sprouting angiogenesis, ACS Appl. Mater. Interfaces 15 (12) (2023) 15047–15058.
[35] P.A. Netti, D.A. Berk, M.A. Swartz, A.J. Grodzinsky, R.K. Jain, Role of extracellular matrix assembly in interstitial transport in solid tumors, Cancer Res. 60 (9) (2000) 2497–2503.
[36] H. Wiig, K. Aukland, O. Tenstad, Isolation of interstitial fluid from rat mammary tumors by a centrifugation method, Am. J. Physiol. Heart Circ. Physiol. 284 (1) (2003) H416–H424.
[37] K.E. Sung, G. Su, C. Pehlke, S.M. Trier, K.W. Eliceiri, P.J. Keely, A. Friedl, D.J. Beebe, Control of 3-dimensional collagen matrix polymerization for reproducible human mammary fibroblast cell culture in microfluidic devices, Biomaterials 30 (27) (2009) 4833–4841.
[38] S.P. Lake, E.S. Hald, V.H. Barocas, Collagen-agarose co-gels as a model for collagen-matrix interaction in soft tissues subjected to indentation, J. Biomed. Mater. Res. A 99 (4) (2011) 507–515.
[39] J.R. Levick, Flow through interstitium and other fibrous matrices, Q. J. Exp. Physiol. 72 (4) (1987) 409–437.
[40] A.M. Hammer, G.M. Sizemore, V.C. Shukla, A. Avendano, S.T. Sizemore, J.J. Chang, R.D. Kladney, M.C. Cuitino, K.A. Thies, Q. Verfurth, A. Chakravarti, L.D. Yee, G. Leone, J.W. Song, S.N. Ghadiali, M.C. Ostrowski, Stromal PDGFR-alpha activation enhances matrix stiffness, impedes mammary ductal development, and accelerates tumor growth, Neoplasia 19 (6) (2017) 496–508.

[41] N.R. Lang, S. Munster, C. Metzner, P. Krauss, S. Schurmann, J. Lange, K.E. Aifantis, O. Friedrich, B. Fabry, Estimating the 3D pore size distribution of biopolymer networks from directionally biased data, Biophys. J. 105 (9) (2013) 1967–1975.
[42] J. Zhu, L.J. Kaufman, Collagen I self-assembly: revealing the developing structures that generate turbidity, Biophys. J. 106 (8) (2014) 1822–1831.
[43] A. Micsonai, F. Wien, E. Bulyaki, J. Kun, E. Moussong, Y.H. Lee, Y. Goto, M. Refregiers, J. Kardos, BeStSel: a web server for accurate protein secondary structure prediction and fold recognition from the circular dichroism spectra, Nucleic. Acids. Res. 46 (W1) (2018) W315–W322.
[44] K. Mandal, Z. Gong, A. Rylander, V.B. Shenoy, P.A. Janmey, Opposite responses of normal hepatocytes and hepatocellular carcinoma cells to substrate viscoelasticity, Biomater. Sci. 8 (5) (2020) 1316–1328.
[45] E.A. Swabb, J. Wei, P.M. Gullino, Diffusion and convection in normal and neoplastic tissues1, Cancer Res. 34 (10) (1974) 2814–2822.
[46] A. Avendano, M. Cortes-Medina, J.W. Song, Application of 3-D microfluidic models for studying mass transport properties of the tumor interstitial matrix, Front. Bioeng. Biotechnol. 7 (2019) 6.
[47] E. Derosa, C. Borselli, P. Netti, Transport of large molecules in hyaluronic acid-based membranes and solution, J. Memb. Sci. 273 (1–2) (2006) 84–88.
[48] A.J. Kvist, A.E. Johnson, M. Morgelin, E. Gustafsson, E. Bengtsson, K. Lindblom, A. Aszodi, R. Fassler, T. Sasaki, R. Timpl, A. Aspberg, Chondroitin sulfate perlecan enhances collagen fibril formation. Implications for perlecan chondrodysplasias, J. Biol. Chem. 281 (44) (2006) 33127–33139.
[49] G.C. Wood, The formation of fibrils from collagen solutions. 3. Effect of chondroitin sulphate and some other naturally occurring polyanions on the rate of formation, Biochem. J. 75 (3) (1960) 605–612.
[50] B.R. Williams, R.A. Gelman, D.C. Poppke, K.A. Piez, Collagen fibril formation. Optimal in vitro conditions and preliminary kinetic results, J. Biol. Chem. 253 (18) (1978) 6578–6585.
[51] B.A. Wallace, The role of circular dichroism spectroscopy in the era of integrative structural biology, Curr. Opin. Struct. Biol. 58 (2019) 191–196.
[52] K.E. Drzewiecki, D.R. Grisham, A.S. Parmar, V. Nanda, D.I. Shreiber, Circular dichroism spectroscopy of collagen fibrillogenesis: a new use for an old technique, Biophys. J. 111 (11) (2016) 2377–2386.
[53] B.R. Williams, R.A. Gelman, D.C. Poppke, K.A. Piez, Collagen fibril formation. Optimal in vitro conditions and preliminary kinetic results, J. Biol. Chem. 253 (18) (1978) 6578–6585.
[54] T. Douglas, S. Heinemann, C. Mietrach, U. Hempel, S. Bierbaum, D. Scharnweber, H. Worch, Interactions of collagen types I and II with chondroitin sulfates A-C and their effect on osteoblast adhesion, Biomacromolecules 8 (4) (2007) 1085–1092.
[55] S.D. Vallet, O. Clerc, S. Ricard-Blum, Glycosaminoglycan-protein interactions: the first draft of the glycosaminoglycan interactome, J. Histochem. Cytochem. 69 (2) (2021) 93–104.
[56] B. Obrink, A study of the interactions between monomeric tropocollagen and glycosaminoglycans, Eur. J. Biochem. 33 (2) (1973) 387–400.
[57] S.D. Vallet, C. Berthollier, S. Ricard-Blum, The glycosaminoglycan interactome 2.0, Am. J. Physiol. Cell Physiol. 322 (6) (2022) C1271–C1278.
[58] C.L. Martin, M.R. Bergman, P.A. Sullivan, L.F. Deravi, Investigating the thermodynamics underlying monosaccharide-mediated collagen polymerization for materials design, Chem. Mater. 34 (7) (2022) 3099–3108.
[59] M. Mihajlovic, M. Rikkers, M. Mihajlovic, M. Viola, G. Schuiringa, B.C. Ilochonwu, R. Masereeuw, L. Vonk, J. Malda, K. Ito, T. Vermonden, Viscoelastic chondroitin sulfate and hyaluronic acid double-network hydrogels with reversible cross-links, Biomacromolecules 23 (3) (2022) 1350–1365.
[60] S. Samantray, O.O. Olubiyi, B. Strodel, The influences of sulphation, salt type, and salt concentration on the structural heterogeneity of glycosaminoglycans, Int. J. Mol. Sci. 22 (21) (2021).
[61] Angiogenesis Inhibitors - National Cancer Institute, 2018. https://www.cancer.gov/about-cancer/treatment/types/immunotherapy/angiogenesis-inhibitors-fact-sheet.
[62] L. Han, A.J. Grodzinsky, C. Ortiz, Nanomechanics of the cartilage extracellular matrix, Annu. Rev. Mater. Res. 41 (2011) 133–168.
[63] Y.S. Pek, M. Spector, I.V. Yannas, L.J. Gibson, Degradation of a collagen-chondroitin-6-sulfate matrix by collagenase and by chondroitinase, Biomaterials 25 (3) (2004) 473–482.
[64] M. Wu, M. Cao, Y. He, Y. Liu, C. Yang, Y. Du, W. Wang, F. Gao, A novel role of low molecular weight hyaluronan in breast cancer metastasis, FASEB J. 29 (4) (2015) 1290–1298.
[65] S.R. Unnikandam Veettil, D. Hwang, J. Correia, M.D. Bartlett, I.C. Schneider, Cancer cell migration in collagen-hyaluronan composite extracellular matrices, Acta Biomater. 130 (2021) 183–198.
[66] Y. Ran, W. Su, L. Ma, X. Wang, X. Li, Insight into the effect of sulfonated chitosan on the structure, rheology and fibrillogenesis of collagen, Int. J. Biol. Macromol. 166 (2021) 1480–1490.
[67] M.A. Swartz, M.E. Fleury, Interstitial flow and its effects in soft tissues, Annu. Rev. Biomed. Eng. 9 (1) (2007) 229–256.
[68] J. Happel, Viscous flow relative to arrays of cylinders, Aiche J. 5 (2) (1959) 174–177.
[69] M.M. Vaeyens, A. Jorge-Penas, J. Barrasa-Fano, C. Steuwe, T. Heck, P. Carmeliet, M. Roeffaers, H. Van Oosterwyck, Matrix deformations around angiogenic sprouts correlate to sprout dynamics and suggest pulling activity, Angiogenesis 23 (3) (2020) 315–324.
[70] W.Y. Wang, E.H. Jarman, D. Lin, B.M. Baker, Dynamic endothelial stalk cell-matrix interactions regulate angiogenic sprout diameter, Front. Bioeng. Biotechnol. 9 (2021) 620128.
[71] J.A. Pedersen, F. Boschetti, M.A. Swartz, Effects of extracellular fiber architecture on cell membrane shear stress in a 3D fibrous matrix, J. Biomech. 40 (7) (2007) 1484–1492.
[72] B. Zhang, L. Chi, Chondroitin sulfate/dermatan sulfate-protein interactions and their biological functions in human diseases: implications and analytical tools, Front. Cell Dev. Biol. 9 (2021) 693563.
[73] L.M. Delgado, Y. Bayon, A. Pandit, D.I. Zeugolis, To cross-link or not to cross-link? Cross-linking associated foreign body response of collagen-based devices, Tissue Eng. Part B 21 (3) (2015) 298–313.
[74] B.N. Mason, A. Starchenko, R.M. Williams, L.J. Bonassar, C.A. Reinhart-King, Tuning three-dimensional collagen matrix stiffness independently of collagen concentration modulates endothelial cell behavior, Acta Biomater. 9 (1) (2013) 4635–4644.
[75] C. Liu, D. Lewin Mejia, B. Chiang, K.E. Luker, G.D. Luker, Hybrid collagen alginate hydrogel as a platform for 3D tumor spheroid invasion, Acta Biomater. 75 (2018) 213–225.
[76] J.E. Prata, T.A. Barth, S.A. Bencherif, N.R. Washburn, Complex fluids based on methacrylated hyaluronic acid, Biomacromolecules 11 (3) (2010) 769–775.
[77] Q. Xu, J.E. Torres, M. Hakim, P.M. Babiak, P. Pal, C.M. Battistoni, M. Nguyen, A. Panitch, L. Solorio, J.C. Liu, Collagen- and hyaluronic acid-based hydrogels and their biomedical applications, Mater. Sci. Eng. R 146 (2021) 100641.